Keratinocyte-associated protein 2 is a bona fide subunit of the mammalian oligosaccharyltransferase

Peristera Roboti and Stephen High*

Faculty of Life Sciences, The University of Manchester, Michael Smith Building, Oxford Road, Manchester, M13 9PT, UK

*Author for correspondence (stephen.high@manchester.ac.uk)

Accepted 25 July 2011
Journal of Cell Science 125, 220–232

doi: 10.1242/jcs.094599

Summary

The oligosaccharyltransferase (OST) complex catalyses the *N*-glycosylation of polypeptides entering the endoplasmic reticulum, a process essential for the productive folding and trafficking of many secretory and membrane proteins. In eukaryotes, the OST typically comprises a homologous catalytic STT3 subunit complexed with several additional components that are usually conserved, and that often function to modulate *N*-glycosylation efficiency. By these criteria, the status of keratinocyte-associated protein 2 (KCP2) was unclear: it was found to co-purify with the canine OST suggesting it is part of the complex but, unlike most other subunits, no potential homologues are apparent in *Saccharomyces cerevisiae*. In this study we have characterised human KCP2 and show that the predominant species results from an alternative initiation of translation to form an integral membrane protein with three transmembrane spans. KCP2 localises to the endoplasmic reticulum, consistent with a role in protein biosynthesis, and has a functional KKxx retrieval signal at its cytosolic C-terminus. Native gel analysis suggests that the majority of KCP2 assembles into a distinct ~500 kDa complex that also contains several bona fide OST subunits, most notably the catalytic STT3A isoform. Co-immunoprecipitation studies confirmed a robust and specific physical interaction between KCP2 and STT3A, and revealed weaker associations with both STT3B and OST48. Taken together, these data strongly support the proposal that KCP2 is a newly identified subunit of the *N*-glycosylation machinery present in a subset of eukaryotes.

Key words: Alternative translation initiation, Endoplasmic reticulum, KKxx motif, *N*-glycosylation, Protein synthesis, Transmembrane topology

Introduction

Asparagine-linked glycosylation (*N*-glycosylation) influences protein folding, quality control, intracellular trafficking and secretion (Hebert et al., 2005; Helenius and Aebi, 2004). It is the most prevalent modification of proteins that traverse the eukaryotic secretory pathway (Apweiler et al., 1999), and defects in this process lead to impaired protein function and disease (Ohtsubo and Marth, 2006). *N*-glycosylation is catalysed by the oligosaccharyltransferase (OST), an integral membrane protein complex active on the lumenal face of the endoplasmic reticulum (ER) that transfers a high-mannose oligosaccharide to asparagines in selected glycosylation sequons (N-x-S/T; x≠P) of nascent polypeptide chains (Kelleher and Gilmore, 2006; Knauer and Lehle, 1999). The association of the OST with membrane-bound ribosomes and the Sec61 translocon, indicates that *N*-glycosylation is functionally coupled with protein translation and translocation (Chavan et al., 2005; Harada et al., 2009; Nikonov et al., 2002). This would ensure that sequons are instantly accessible to the OST and less likely to be masked by partial folding of the polypeptide inside the ER (Kowarik et al., 2006; Ruiz-Canada et al., 2009; Schulz et al., 2009). Nevertheless, the mammalian OST can also mediate the post-translational *N*-glycosylation of particular sequons (Bolt et al., 2005; Kolhekar et al., 1998; Ruiz-Canada et al., 2009).

Although some protozoa utilise comparatively simple, single-component OST complexes (Hese et al., 2009; Izquierdo et al., 2009; Nasab et al., 2008), many eukaryotes possess multicomponent OSTs that appear relatively conserved (Kelleher and Gilmore, 2006). The yeast OST consists of eight non-identical membrane protein subunits (Stt3p, Ost1p, Swp1p, Wbp1p, Ost2p, Ost4p, Ost5p and either one of the two homologues, Ost3p or Ost6p) that associate in vivo to form a catalytically active complex (Karaoglu et al., 1997; te Heesen et al., 1993; Yan et al., 2003). Although various studies have identified several mammalian OST subunits on the basis of both in vitro function and homology with their yeast counterparts (Kelleher and Gilmore, 2006) (see also supplementary material Fig. S1) the exact composition and organisation of the mammalian OST is less well defined. Furthermore, mammalian cells express two homologues of yeast Stt3p, STT3A and STT3B, both of which are capable of in vitro oligosaccharide donor and peptide acceptor binding (Kelleher et al., 2003), and catalysis of *N*-glycosylation (Nilsson et al., 2003). As a result, two distinct OST isoforms have been described; the STT3A isoform has been shown to be less active, but highly selective towards fully assembled oligosaccharide donors than the STT3B isoform (Kelleher et al., 2003). However, by acting primarily at different stages of glycoprotein synthesis, it has been proposed that the two OST isoforms have complementary roles in order to maximise the efficiency of protein *N*-glycosylation (Ruiz-Canada et al., 2009).

Previous studies of both yeast and mammalian OST proteins have suggested that some of the non-catalytic subunits are required for the assembly and the stability of the functional complex. Hence, DAD1 (Ost2p in yeast) is important for structural integrity, and its loss destabilises the complex,

resulting in decreased OST activity and ultimately in cell death (Kelleher and Gilmore, 1997; Sanjay et al., 1998; Silberstein et al., 1995). Other non-catalytic subunits contribute to the efficiency of the *N*-glycosylation process. OST48 (Wbp1p) is suggested to recognise the oligosaccharide donor substrate, ensuring its supply to the active site (Bause et al., 1997; Beatson and Ponting, 2004; Kelleher et al., 1992; Pathak et al., 1995), and ribophorin I (Ost1p) presents a subset of membrane proteins to the OST catalytic core (Wilson and High, 2007; Wilson et al., 2008). In yeast, Ost3p and Ost6p enhance the *N*-glycosylation of defined sequons (Schulz and Aebi, 2009; Schulz et al., 2009; Spirig et al., 2005), whereas Ost4p might have a role in recruiting either Ost3p or Ost6p into yeast OST (Spirig et al., 2005). The roles of their mammalian equivalents (supplementary material Fig. S1) are unclear at present.

A proteomic study revealed two poorly characterised proteins, DC2 (also known as OSTC) and keratinocyte-associated protein 2 (KCP2; also known as KRTCAP2), that co-purified with the mammalian OST under defined conditions, suggesting that these components represent previously unknown OST subunits (Shibatani et al., 2005). DC2 is weakly homologous to the C-terminal domain of yeast Ost3p and Ost6p, and could therefore influence nascent polypeptide *N*-glycosylation (see above). By contrast, a search for conserved domains in KCP2 found no homology to known protein families, and its potential function remains unclear. Interestingly, KCP2 mRNA levels appear high in tissues active in secretion, such as the pancreas and liver (Bonkobara et al., 2003), suggesting that KCP2 expression is associated with a demand for increased glycoprotein synthesis, but this issue has not been further addressed (cf. Shibatani et al., 2005).

We have characterised KCP2 with respect to its membrane topology, subcellular localisation and physical associations. We identified native human KCP2 to be the product of alternative translation initiation, and show that it is a triple-spanning membrane protein with a classical cytosolic C-terminal di-lysine motif that contributes to its ER localisation. Analysis of the mammalian OST by blue native polyacrylamide gel electrophoresis (BN-PAGE) confirmed that KCP2 co-migrates with several other components of the native OST complex, and suggests that it is preferentially incorporated into STT3A-containing OST isoforms. By contrast, we found evidence that DC2 is associated with both STT3A and STT3B OST isoforms by BN-PAGE. Compellingly, co-immunoprecipitation studies revealed a specific interaction between KCP2 and both exogenous STT3A and endogenous OST48. We also observed an interaction of KCP2 with exogenous STT3B, albeit at a quantitatively lower level than with STT3A. We conclude that KCP2 is a bona fide subunit of both mammalian OST isoforms that preferentially associates with the 'co-translational' STT3A isoform.

Results

Sequence features of KCP2

The predicted open reading frame of the human *KCP2* gene encodes a 162-amino-acid polypeptide with an expected mass of ~18 kDa. Hydropathy modelling using several programs, including TMpred (Hofmann and Stoffel, 1993) and SOSUI (Hirokawa et al., 1998), has suggested KCP2 is an integral membrane protein with three transmembrane (TM) domains (Fig. 1, TM1–TM3). However, the TMHMM algorithm (Sonnhammer et al., 1998) has predicted the final hydrophobic stretch as two short TM domains, resulting in a model with four TM spans. Amino acid sequence alignments with KCP2 family members from other species showed that the region N-terminal of the first predicted TM span is especially divergent and of variable length (Fig. 1; supplementary material Fig. S2). By contrast, the remaining amino acid sequence is highly conserved, and appears to contain a classical ER localisation motif of the KKxx type (Fig. 1; supplementary material Fig. S2) that typically retains membrane proteins at the ER (Teasdale and Jackson, 1996).

Authentic human KCP2 results from alternative initiation

Analysis of endogenous KCP2 expression in canine pancreatic microsomes and human embryonic kidney (HEK) 293 cells with an anti-KCP2 antibody recognising the relatively conserved C-terminal region of the protein (see Fig. 1) showed that canine and human KCP2 co-migrate as ~15 kDa species (Fig. 2A, αKCP2 panel, cf. lanes 1 and 2), despite the large predicted difference in their respective coding regions (136 and 162 amino acids; see Fig. 1). One obvious explanation for this behaviour is that human KCP2 is in fact similar to the canine protein. Because both proteins must contain the C-terminal epitope recognised by the antibody, we concluded that the initiation of translation of the human mRNA probably does not occur at the first start codon present, but rather at a downstream AUG codon [methionine (Met)26 or Met27; Fig. 2B] comparable with the predicted start of the shorter canine protein (see Fig. 1).

To elucidate the identity of the human ~15 kDa KCP2 species, the full-length coding region (Met1 KCP2; Fig. 2B) was transiently expressed in HEK293 cells and compared with the product of the open reading frame lacking the first AUG but preserving those at codons 26 and 27 (Met26/27 KCP2; Fig. 2B). Analysis with the anti-KCP2 antibody showed that in both cases this resulted in a substantial increase in the level of the ~15 kDa species compared with the endogenous level in control cells (Fig. 2A, αKCP2 panel, cf. lanes 2, 3 and 6). Expression of Met1 KCP2 additionally revealed low levels of a larger KCP2 species of ~18 kDa (Fig. 2A, αKCP2 panel, lane 3, white asterisk), presumably resulting from inefficient initiation at the first AUG codon. To further test the origin of the two KCP2-derived species observed upon transient expression, a FLAG tag was introduced immediately after the Met1 codon (Met1 FLAGKCP2; Fig. 2B). This resulted in a higher level of an even larger ~19 kDa KCP2-derived product (Fig. 2A, αKCP2 panel, cf. lanes 3 and 4) in addition to an increase in the ~15 kDa product (Fig. 2A, αKCP2 panel, cf. lanes 2–4). The ~19 kDa product contained the FLAG epitope, whereas the ~15 kDa product did not (Fig. 2A, merged panel, lane 4). The higher levels of the ~19 kDa product are consistent with an improvement in the surrounding context of the first AUG codon, resulting from the introduction of the FLAG tag (Fig. 2C).

The products of translational initiation at Met26 or Met27 are indistinguishable by SDS-PAGE, and therefore the precise AUG codon at which protein synthesis is normally initiated could not be determined by immunoblotting of the products. Examination of the KCP2 coding sequence revealed the context of the Met1 AUG codon to be clearly suboptimal (Kozak, 1991) when compared with those downstream at Met26 or Met27 (Fig. 2C). This is consistent with initiation at one or more of these two locations resulting from 'leaky' ribosome scanning of *KCP2* mRNA (Kozak, 2002). Consistent with this suggestion, when the

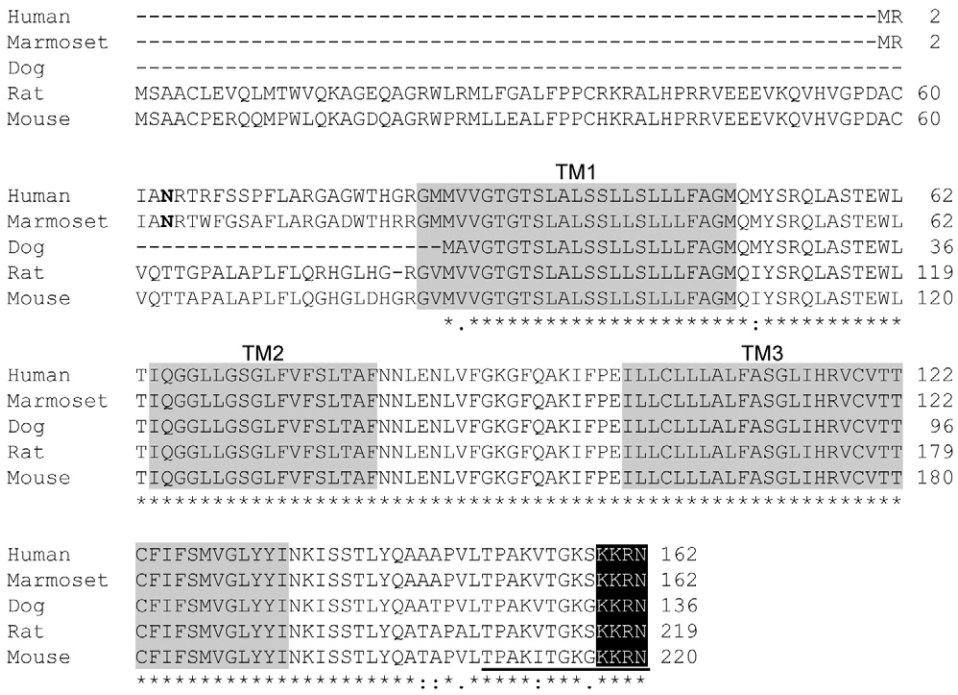

Fig. 1. KCP2 is a putative polytopic membrane protein with conserved sequence features. Predicted amino acid sequences of KCP2 from human (Ensembl Gene ID ENSG00000163463), marmoset (Ensembl Gene ID ENSCJAG00000009017), dog (Ensembl Gene ID ENSCAFG00000017055), rat (Ensembl Gene ID ENSRNOG00000020542) and mouse (Ensembl Gene ID ENSMUSG00000042747) were obtained from the Ensembl Genome Browser (http://www.ensembl.org/index.html) and aligned using ClustalW2. Residues are numbered relative to the presumptive initiating Met (on the right). Identical residues are denoted with an asterisk, closely related residues with a colon and less conserved residues with a full stop. Putative TM spans (TM1–TM3) are shaded in grey and a potential di-lysine motif at the extreme C-terminus is indicated by white letters on a black background. The Asn residues, shown in bold in the human and marmoset sequences, are single potential *N*-glycosylation sites (cf. supplementary material Fig. S2). The underlined sequence is the segment of the mouse protein used to produce KCP2-specific antibodies.

KCP2 open reading frame employing an improved AUG context was expressed (KozakMet1 KCP2; Fig. 2C), this resulted in a substantial increase in the level of the ~18 kDa product (Fig. 2A, αKCP2 panel, cf. lanes 3 and 5).

Taken together, these results suggest that the ~15 kDa version of KCP2 is the predominant form expressed in most mammalian cells (see below), and we will henceforth refer to this protein as KCP2 (Fig. 2A, merged panel, KCP2). Given that Met27 is highly conserved in a range of species (supplementary material Fig. S2), and the flanking sequence surrounding Met27 provides an optimal context for initiation (Fig. 2C), we added a FLAG epitope tag after Met27 (Met27 FLAGKCP2; Fig. 2B) to facilitate subsequent analysis. The resulting protein was efficiently expressed (Fig. 2A, merged panel, cf. lanes 2 and 7, FLAGKCP2), and the location of the tag just before the predicted TM1 was unlikely to perturb its targeting to, or folding at, the ER membrane.

KCP2 is inserted in the ER membrane with its N-terminus in the ER lumen and its C-terminus in the cytosol

As outlined above, the hydrophobicity profile of KCP2 suggests at least three hydrophobic domains, each of sufficient length to span the membrane bilayer (Fig. 3A). If this prediction is correct, and if the C-terminal di-lysine motif functions as a cytosolic ER retention or retrieval signal (Teasdale and Jackson, 1996), the N-terminus of the protein would face the ER lumen (cf. Fig. 3B, FLAGKCP2). To examine the actual membrane topology of KCP2, we performed a trypsin protection assay using HeLa cells expressing FLAG–KCP2 (Met27 FLAGKCP2, see Fig. 2) that were semi-permeabilised with a low concentration of digitonin (Fig. 3C). Under these conditions, digitonin preferentially permeabilises the plasma membrane (Wilson et al., 1995), allowing the selective detection of cytosolic epitopes present on intracellular membrane proteins. Samples of the protease-treated cellular material were subjected to immunoblot analysis with antibodies to either the N-terminal FLAG epitope or the C-terminal KCP2 epitope (Fig. 3B, FLAGKCP2). Both antibodies recognised FLAG–KCP2 as a ~16 kDa protein in the non-digested membrane sample (Fig. 3C, merged panel, lane 1, FLAGKCP2). By contrast, the endogenous protein was observed as a slightly smaller protein of ~15 kDa that co-migrated with the canine version present in ER microsomes, and was detected only by the αKCP2 antibody (Fig. 3C, αKCP2 panel, lane 1, KCP2; see also Fig. 2A). Following proteolysis of digitonin-treated cells with trypsin, the endogenous KCP2 was completely absent and the FLAG–KCP2 signal greatly diminished at the shortest time point analysed (Fig. 3C, αKCP2 panel, lanes 2–5), suggesting that the C-terminal KCP2 epitope is exposed to the cytosol and digested by trypsin. The anti-FLAG antibody detected a Triton-X-100-sensitive proteolytic fragment of FLAG–KCP2 (Fig. 3C, αFLAG panel, lanes 2–5, FLAGKCP2ΔC), indicating that the FLAG epitope was protected by the ER membrane and hence in the ER lumen. The C-terminal hydrophilic region of KCP2 contains several potential cleavage sites for trypsin (Fig. 1 and Fig. 3B,

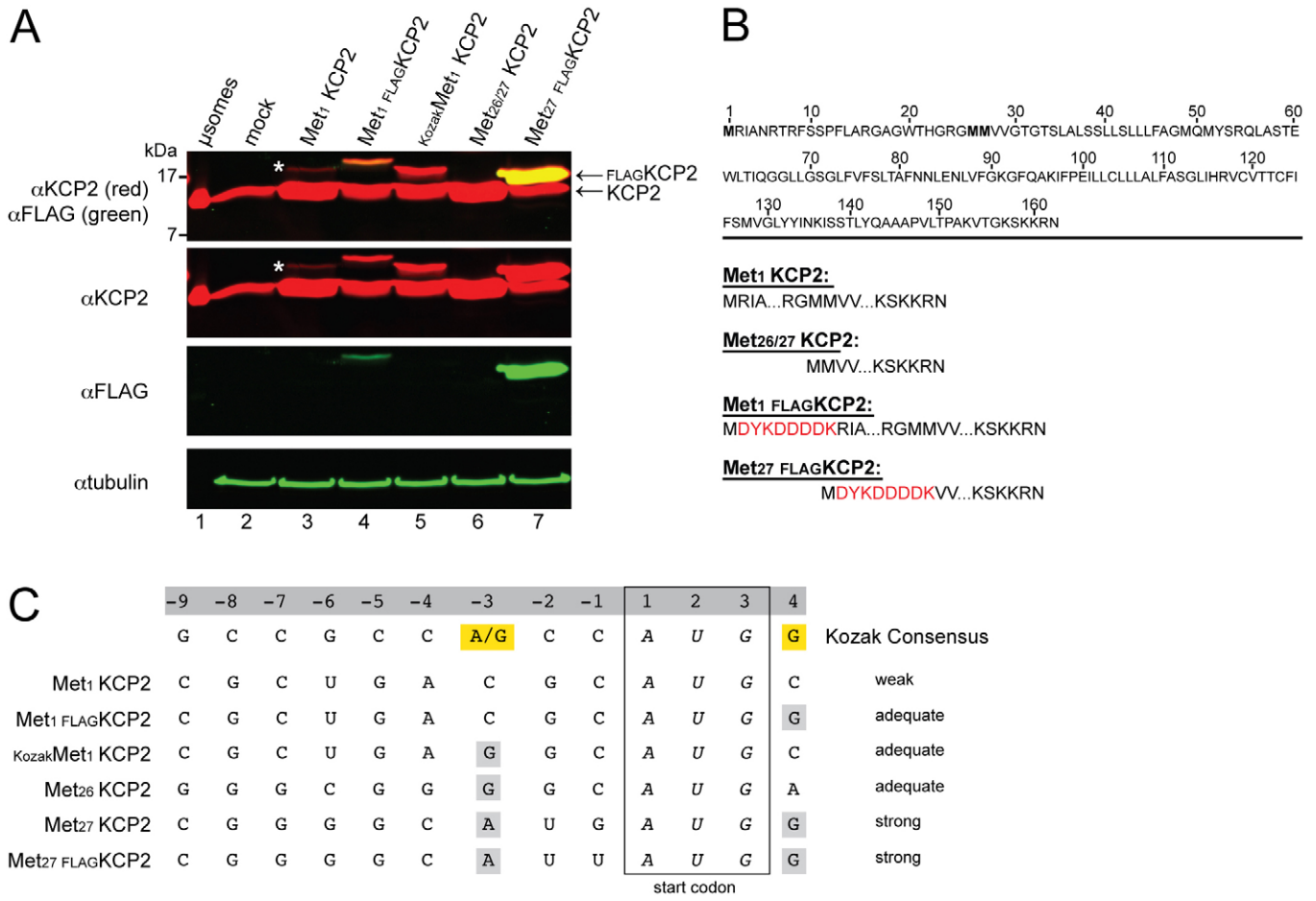

Fig. 2. N-terminally truncated KCP2 is the predominant form expressed in cells. (**A**) HEK293 cells were transfected with an empty vector (mock) or constructs expressing full-length human KCP2 (Met1 KCP2), N-terminal FLAG-tagged full-length KCP2 (Met1 FLAGKCP2), full-length KCP2 with a Kozak consensus sequence engineered to precede Met1 (KozakMet1 KCP2), a KCP2 variant that lacks the first initiation codon Met26/27 KCP2, and a N-terminal FLAG-tagged KCP2 variant that lacks both Met1 and Met26 (Met27 FLAGKCP2). Triton X-100 lysates were prepared and analysed by immunoblotting with antibodies against the C-terminus of KCP2 (αKCP2) and the N-terminal FLAG epitope (αFLAG). Anti-KCP2 rabbit polyclonal and anti-FLAG mouse monoclonal antibodies were visualised using IRDye680-conjugated anti-rabbit IgG (red) and IRDye800-conjugated anti-mouse IgG (green) secondary antibodies, respectively. Dog pancreatic microsomes were also analysed as indicated above. (**B**) The amino acid sequence of human KCP2 features three potential in-frame translation initiation sites (M1, M26 and M27), which are indicated in bold. The KCP2 constructs used in the present study are outlined with the FLAG epitope shown in red. Note that Met1 KCP2 contains all three potential initiation methionines, whereas Met1 is mutated to Ile within Met26/27 KCP2 resulting in translation initiation from the downstream in-frame methionine, Met26 and/or Met27. Both Met1 and Met26 are mutated to Ile within the Met27 FLAG–KCP2 construct encoding a KCP2 variant beginning obligatorily at Met27. (**C**) Comparison between the eukaryotic Kozak consensus sequence and the mRNA sequences flanking the first (Met1) and downstream (Met26, Met27) putative translation start sites. Nucleotides important for efficient translation initiation are highlighted in yellow, and nucleotides matching these elements of the Kozak consensus sequence are shown in grey. Examination of the sequences studied shows that the Met27 site is the closest match to the consensus site.

asterisks), and the slight increase in the mobility of FLAG–KCP2 after trypsin treatment (Fig. 3C, αFLAG panel, cf. lanes 1–4) is consistent with proteolysis at one or more of these sites.

As controls for membrane integrity, endogenous ribophorin I and Grp94 (Fig. 3B, Rib I and Grp94) were monitored in the same samples. Using an antibody specific for the lumenal domain of ribophorin I, a trypsin-dependent product of ~50 kDa was detected (Fig. 3C, αRib I panel, lanes 2–4, Rib IΔC). Furthermore, Grp94 was protected from trypsin digestion (Fig. 3C, αGrp94 panel, lanes 2–4, Grp94). The resistance of Grp94 and the lumenal domain of ribophorin I to proteolysis by trypsin confirms that the ER membrane remained intact after digitonin treatment, but could be disrupted with Triton X-100 (Fig. 3C, αRib I and αGrp94 panels, lane 5). The membrane topology of KCP2 was also addressed by trypsin treatment of in vitro synthesised radiolabelled FLAG–KCP2 and immunoprecipitation analysis with anti-FLAG or anti-KCP2 antibodies (supplementary material Fig. S3). This approach confirmed the orientation of the N- and C-termini deduced from the immunoblot analysis. Taken together, these findings strongly indicate that KCP2 resides in the ER membrane with its N-terminus in the ER lumen and C-terminus in the cytosol, consistent with the prediction of three TM spans (cf. Fig. 3B).

A classical cytosolic C-terminal di-lysine motif contributes to the ER residency of KCP2

One important outcome of empirically determining KCP2 membrane topology is that the highly conserved C-terminal

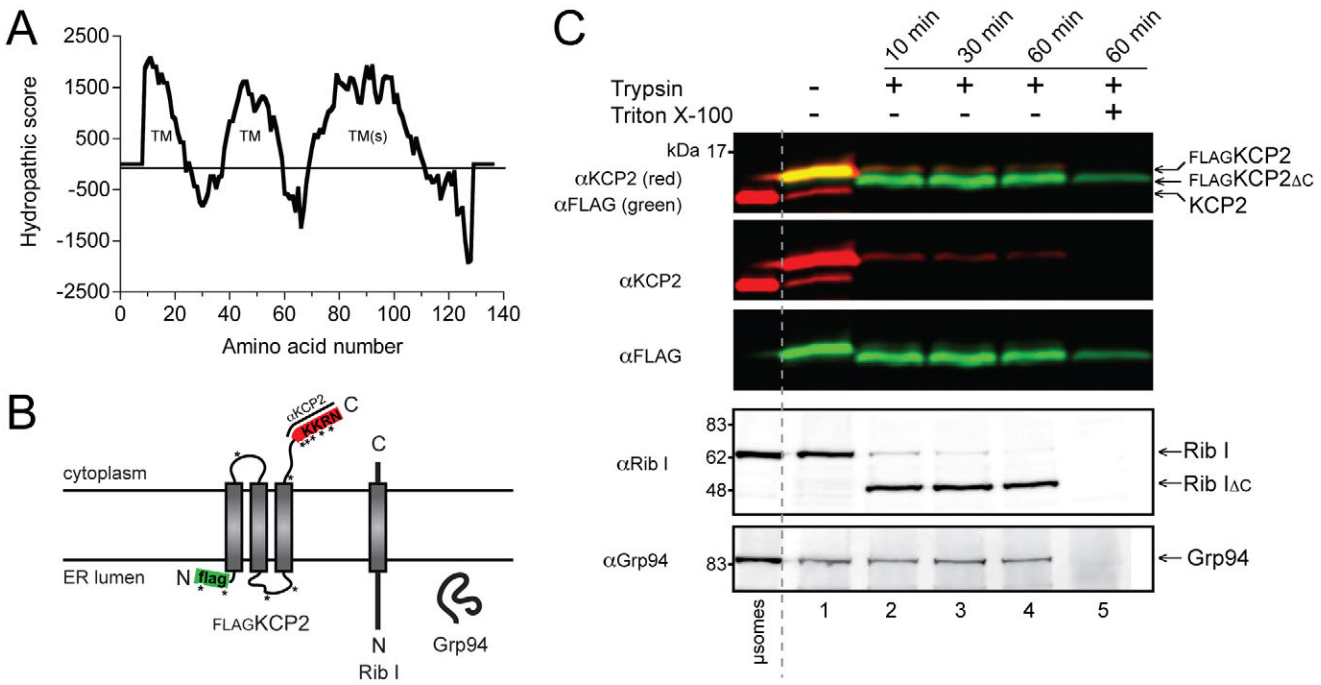

Fig. 3. KCP2 is a triple-spanning membrane protein of the ER with lumenal N-terminal and cytosolic C-terminal domains. (**A**) The human KCP2 amino acid sequence was analysed using the TMpred program (Hofmann and Stoffel, 1993), and a hydropathy profile was produced. Peaks >500 indicate TM-spanning domains. (**B**) Cartoon depicting the most commonly predicted membrane topology of FLAG–KCP2 and the known locations of ribophorin I (Rib I) and Grp94. The position of the anti-KCP2 and anti-FLAG epitopes are shown in red and green, respectively. Potential trypsin sites (Lys and Arg) are indicated by asterisks. (**C**) Experimental verification of KCP2 topology. HeLa cells expressing FLAG–KCP2 were semi-permeabilised with digitonin, and equal aliquots of the isolated membranes were mock-treated or treated with trypsin for increasing periods of time in the presence or absence of 1% Triton X-100. Samples were analysed by immunoblotting with antibodies against the C-terminal (αKCP2) and N-terminal (αFLAG) domains of FLAG–KCP2, the lumenal domain of the ER membrane protein Rib I (αRib I) and against the lumenal ER protein Grp94 (αGrp94).

KKxx motif (supplementary material Fig. S2) is present in the cytosol (Fig. 3B) and thereby available for binding by coat protein I (COPI) components, which function in retrograde transport between the Golgi complex and the ER (Lee et al., 2004). To test the involvement of this di-lysine motif in the ER localisation of KCP2, we produced a mutant form of FLAG–KCP2 with the two lysines of the KKRN sequence replaced by serines (FLAG–KCP2 SSRN) to disrupt COPI binding and perturb potential KKxx-dependent recycling. COS-7 cells were transfected with DNA encoding either wild-type FLAG–KCP2 or FLAG–KCP2 SSRN, and the subcellular distribution of the two proteins was examined by immunofluorescence microscopy. The C-terminal domain of KCP2 was used as the immunogen for the antisera used in this study, and the di-lysine motif clearly contributes to the epitope that is recognised by anti-KCP2 because a substantial reduction in FLAG–KCP2 immunoreactivity was observed (Fig. 4A, αKCP2 panel, cf. lanes 2 and 3). By contrast, there was no effect on the signal obtained using the N-terminal FLAG epitope, confirming that both proteins are expressed at comparable levels (Fig. 4A, αFLAG panel, cf. lanes 2 and 3). In the first instance, anti-FLAG antibodies were used to visualise any N-terminal FLAG epitope present on the extracellular surface of non-permeabilised COS-7 cells (Fig. 4B). We found that neither wild-type FLAG–KCP2 nor FLAG–KCP2 SSRN colocalised with concanavalin A (Con A) bound to cell-surface glycoproteins in non-permeabilised cells (Fig. 4B, non-permeabilised panel), suggesting neither protein is stably expressed at the plasma membrane. In detergent-permeabilised cells, we observed immunostaining of both wild-type and mutant proteins, predominantly this staining appeared to be a reticular network characteristic of the ER (Fig. 4B, permeabilised panel).

To further examine the intracellular distribution of overexpressed FLAG–KCP2 or FLAG–KCP2 SSRN in COS-7 cells, we performed co-staining with the anti-FLAG antibody and antibodies against proteins that are well-defined markers for specific organelles. Wild-type FLAG–KCP2 and FLAG–KCP2 SSRN were detected in a reticular staining pattern that strongly colocalised with the ER marker calnexin (Fig. 5A), confirming their ER localisation. We also noted that expression of both KCP2 derivatives resulted in subtle changes to ER morphology (Fig. 5A, cf. calnexin staining in FLAG-positive and FLAG-negative cells). However, only the mutant variant of KCP2 showed some obvious colocalisation with the *trans* Golgi network (TGN) marker TGN46 (Fig. 5B) (Banting and Ponnambalam, 1997). Taken together, these results indicate that overexpressed wild-type FLAG–KCP2 is efficiently retained in the ER, whereas a fraction of FLAG–KCP2 SSRN can escape the ER and reach distal locations within the secretory pathway. We can exclude the possibility that a proportion of FLAG–KCP2 SSRN escaped the ER as a result of overloading the endogenous retention–retrieval machineries, because the anti-FLAG antibody detected similar expression levels for both wild-type FLAG–KCP2 and FLAG–KCP2 SSRN (Fig. 4A, αFLAG panel, cf. lanes 2 and 3). Taken together, we conclude that the KKRN sequence at the cytoplasmic C-terminus of KCP2 contributes to its ER localisation.

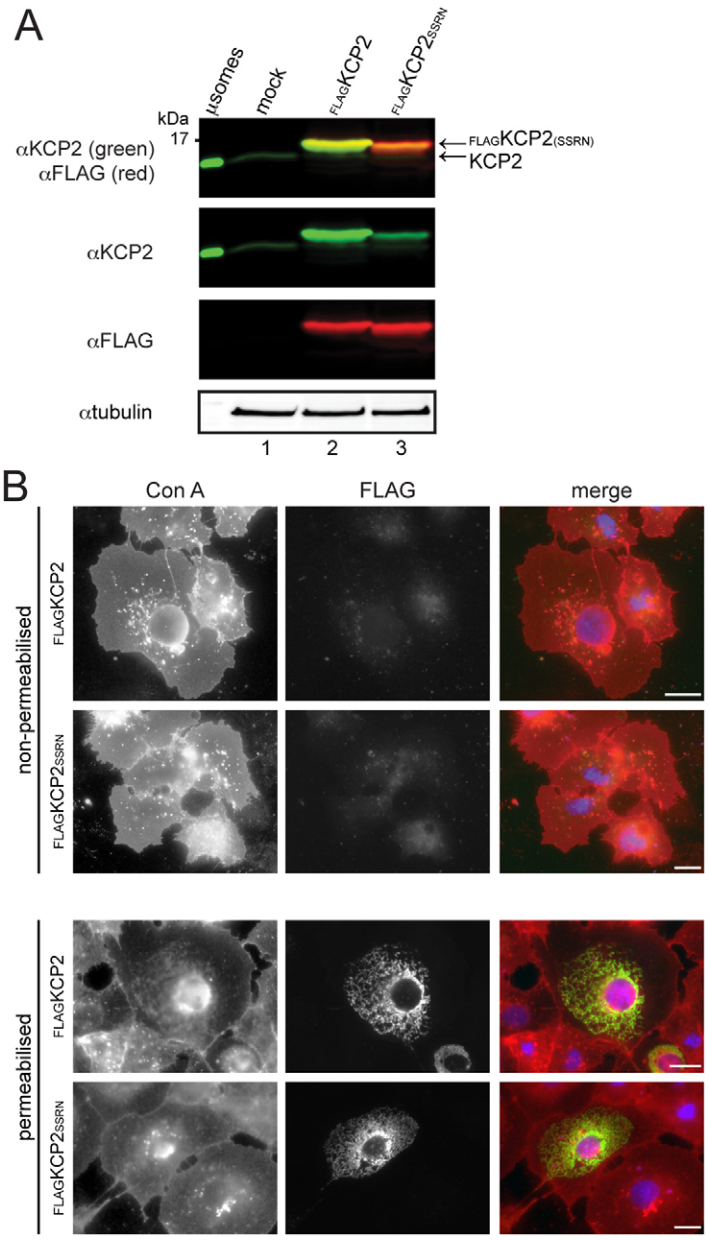

Fig. 4. Mutation of the cytoplasmic di-lysine motif does not allow the escape of KCP2 to the cell surface. (**A**) COS-7 cells were mock-transfected, or transfected with DNA encoding either wild-type FLAG–KCP2 or its mutant variant FLAG–KCP2 SSRN. Triton X-100 lysates were prepared and analysed by immunoblotting using antibodies against the C-terminal domain of KCP2 (αKCP2) and against the N-terminal FLAG epitope (αFLAG). Tubulin was monitored as a loading control. (**B**) COS-7 cells expressing either wild-type FLAG–KCP2 or FLAG–KCP2 SSRN were fixed, and permeabilised with detergent or left untreated, before staining with the anti-FLAG antibody (green) to detect intracellular and cell-surface expression, respectively. In each case, staining of the cells with fluorescently modified Con A (red) was performed before permeabilisation to label cell-surface glycoproteins. The cells shown are representative of transfected cells. Scale bars: 10 μm.

KCP2 and the catalytic STT3A subunit of the OST exhibit similar ribosome affinities

In order to facilitate co-translational *N*-glycosylation of newly synthesised proteins, OST complexes are adjacent to active ER translocation channels (Harada et al., 2009; Shibatani et al., 2005). KCP2 has been shown to co-purify with the mammalian OST complex after puromycin treatment of digitonin-solubilised ribosome–translocon complexes, and on this basis it was hypothesised that it might be a previously unknown OST subunit (Shibatani et al., 2005). It is also well established that OST subunits and ER translocon components form distinct complexes that co-sediment with ribosome-nascent chains as part of the ribosome-associated membrane protein (RAMP) fraction, when the ER is solubilised with non-ionic detergents (Gorlich et al., 1992; Shibatani et al., 2005). In order to compare the behaviour of KCP2 with that of bona fide OST subunits, its association with the RAMP fraction was therefore examined. HeLa cells were solubilised with digitonin at increasing NaCl concentrations, and the resulting samples then centrifuged to separate soluble proteins from RAMPs. The distribution of proteins between the soluble and RAMP fractions was then evaluated by quantitative immunoblotting (Fig. 6). As it is a ribosomal protein, Rpl17, could not be extracted even at the highest salt concentration (Fig. 6, αRpl17). Only ~10% of the Sec61α translocon subunit was present in the supernatant fraction when the cells were solubilised in the presence of 150 mM NaCl (Fig. 6, αSec61α), demonstrating its comparatively tight association with the RAMP fraction. By contrast, several OST subunits were more easily released under the same conditions with 40–50% of STT3B, OST48 and ribophorin I in the soluble pool (Fig. 6, αSTT3B, αOST48 and αRib I). Notably, only ~20% of STT3A and KCP2 were released in the presence of

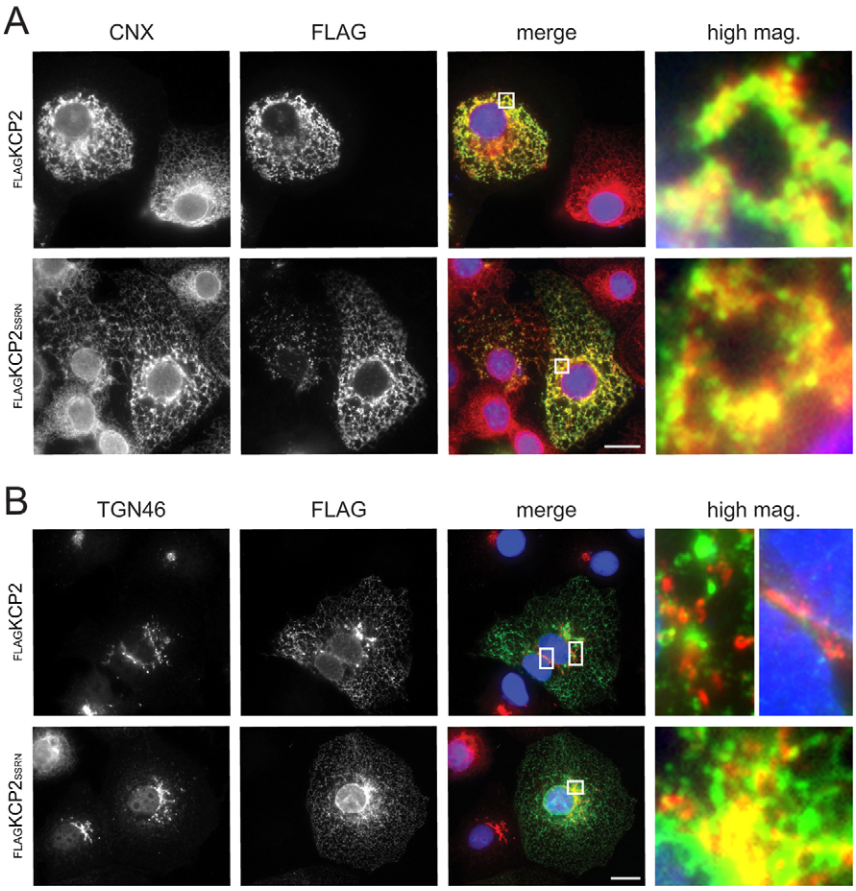

Fig. 5. The cytoplasmic di-lysine motif contributes to the ER localisation of KCP2. COS-7 cells expressing FLAG–KCP2 or FLAG–KCP2 SSRN were fixed, permeabilised and probed with antibodies specific for the FLAG epitope (green) and antibodies against markers (red) of the (**A**) ER (CNX) and (**B**) TGN (TGN46). For each panel, the area indicated by a white box is shown at a higher magnification on the right. Yellow indicates areas of colocalisation. Scale bars: 10 μm.

150 mM NaCl (Fig. 6, αSTT3A and αKCP2). Thus, STT3A and KCP2 show a stronger association with ribosome–translocon complexes than several other OST subunits.

KCP2 assembles with mammalian OST subunits into distinct complexes

As a first step towards exploring any association between KCP2 and the OST complex, we compared the basal expression of KCP2 with known OST subunits in different human cell lines. We detected relatively high levels of KCP2 in HepG2 (hepatoma) cells and HEK293 (kidney) cells compared with HT1080 (fibrosarcoma) cells and HeLa (cervical cancer) cells (Fig. 7A, αKCP2 panel). Interestingly, this pattern correlates better with expression of the STT3A isoform of the OST than that of STT3B (Fig. 7A, cf. αKCP2, αSTT3A and αSTT3B panels). Two other OST subunits, OST48 and DAD1, and the translocon protein Sec61α show a more uniform level of expression when qualitatively compared with the tubulin loading control (Fig. 7A, cf. αKCP2, αDAD1, αOST48 and αSec61α panels). The similarity in the expression profiles of KCP2 and STT3A raised the possibility that the expression and/or function of these two proteins might be linked.

Because HepG2 cells showed a comparatively high level of endogenous KCP2 expression (Fig. 7A), its incorporation into native OST complexes was examined by BN-PAGE analysis (Wittig et al., 2006) of digitonin-solubilised extracts (Fig. 7B). Using BN-PAGE and western blotting, we identified STT3A in at least two distinct complexes of ~470 kDa and ~500 kDa (denoted OSTC470 and OSTC500, respectively; Fig. 7B, lane 3). By contrast, STT3B was present in a larger and more heterologous complex of ~520–580 kDa (OSTC550; Fig. 7B, lane 4). Two previously characterised OST subunits, OST48 and DAD1 co-migrated with both STT3A, present in OSTC470 and OSTC500, and with the larger STT3B-containing OSTC550 (Fig. 7B, lanes 5 and 6). Most significantly, the majority of KCP2 was present in the OSTC500 but not in the smaller OSTC470 (Fig. 7B, lane 2), consistent with the previous observation by Shibatani et al. (Shibatani et al., 2005). Because the STT3B-containing products are diffuse, its potential association with KCP2 is more difficult to assess by BN-PAGE. However, no compelling evidence for discrete co-migrating species containing STT3B and KCP2 was seen (Fig. 7B,C). Immunoblotting with antibodies against DC2, another putative OST component that was detected along with KCP2 by mass spectrometry (Shibatani et al., 2005), revealed clear evidence of its presence in all three OST complexes (Fig. 7C, lane 3). In contrast to these OST subunits, the major ER translocon subunit Sec61α migrated as a much smaller complex (Sec61C; Fig. 7B, lane 1), and was not apparent in the three OST complexes defined here. If the digitonin-stable OST species were treated with SDS before electrophoresis, the complexes were disrupted (Fig. 7B, lane 7).

FLAG–KCP2 physically interacts with core components of the *N*-glycosylation machinery

The previous results obtained by BN-PAGE analysis prompted us to investigate whether KCP2 interacts directly with the catalytic OST subunits, STT3A and STT3B. Endogenous STT3A is difficult to detect efficiently in many mammalian cells (Fig. 7A)

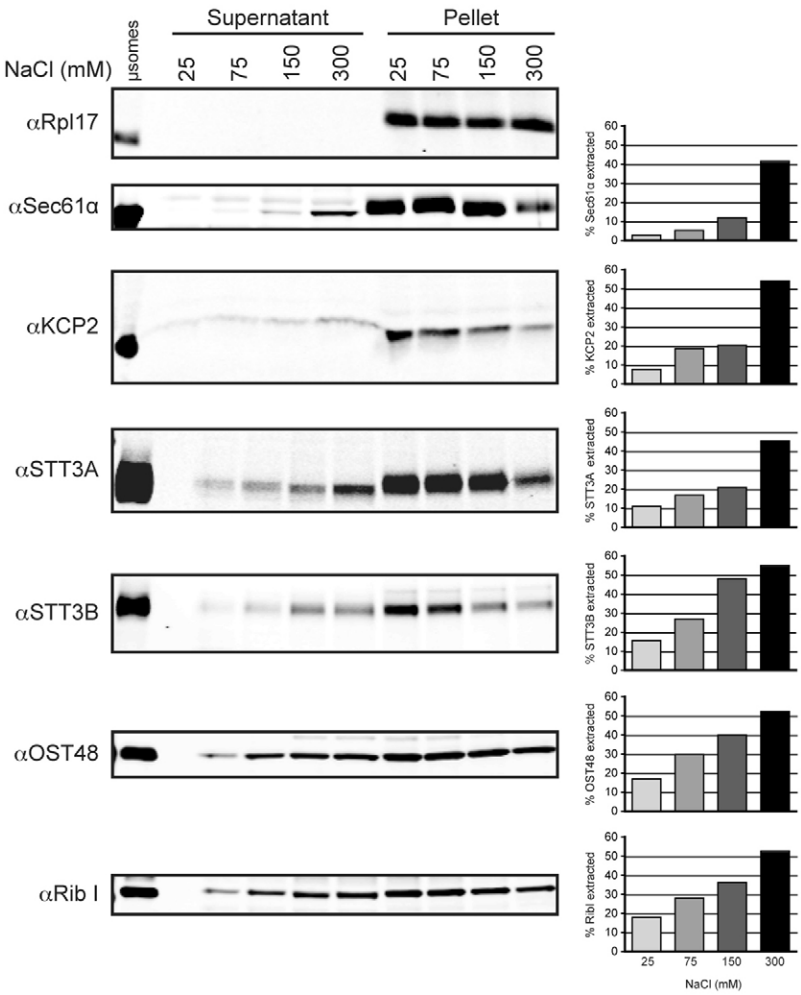

Fig. 6. KCP2 and STT3A are not readily extracted from the RAMP fraction. HeLa cells were solubilised in a buffer containing 1.5% digitonin and adjusted to 25, 75, 150 or 300 mM NaCl. After ultracentrifugation, soluble supernatant fractions and their corresponding RAMP fractions were isolated. The distribution of KCP2, STT3A, STT3B, OST48, Rib I, Sec61α and Rpl17 between these fractions was assessed by infrared fluorescent western blotting. Fluorescent signals were quantified and the amount of extracted protein was expressed as a percentage of total protein for each fraction.

(see also Kelleher et al., 2003), and hence its potential association with KCP2 was analysed by the exogenous expression of both proteins. HEK293 cells were transiently transfected with plasmids encoding FLAG–KCP2 and either STT3A (Fig. 8A) or STT3B (Fig. 8B), solubilised with digitonin, and subjected to native immunoprecipitations to isolate FLAG-tagged species together with interacting components. Immunoblotting with anti-KCP2 revealed the successful recovery of FLAG–KCP2 in the anti-FLAG immunoprecipitates (Fig. 8A,B upper panels, lanes 5 and 6, FLAGKCP2). Although transient transfection had only a modest effect on total levels of STT3A and STT3B (Fig. 8A,B, middle panels – higher sensitivity; cf. lanes 1–3, STT3A/B), a significant proportion of overexpressed STT3A (~70%) co-immunoprecipitated with FLAG–KCP2 (Fig. 8A, upper panel, cf. lanes 3 and 6, STT3A; Fig. 8C). Furthermore, even a fraction of endogenous STT3A (~15%) was isolated in a complex with FLAG–KCP2 (Fig. 8A, middle panel, cf. lanes 4 and 5, STT3A; Fig. 8C). In the case of STT3B, we also found clear evidence of its co-immunoprecipitation with FLAG–KCP2 (Fig. 8B, upper panel, cf. lanes 4–6, STT3B). In this case the proportion of exogenous STT3B associating with FLAG–KCP2 (~15%) was lower than that of STT3A (Fig. 8C), and it was not clear whether any endogenous STT3B was recovered in the pull-down (Fig. 8B, middle panel, cf. lanes 4 and 5, STT3B; Fig. 8C). In addition to its interactions with both catalytic OST subunits, endogenous OST48 was specifically detected in all the anti-FLAG pull-downs (Fig. 8A,B, lower panels, lanes 5 and 6, OST48). Interestingly, the association between FLAG–KCP2 and OST48 was not enhanced by overexpression of either STT3A or STT3B (Fig. 8A,B, lower panels, cf. lanes 5 and 6, OST48), suggesting that this interaction between OST48 and KCP2 is not mediated by STT3A or STT3B.

To control for the specificity of the interactions between KCP2 and the OST subunits described, we performed parallel co-immunoprecipitation experiments with cells overexpressing another FLAG-tagged polytopic ER membrane protein, FLAG–gp78. Although FLAG–gp78 was efficiently immunoprecipitated (Fig. 8D,E, lanes 5 and 6, FLAGgp78), no STT3A, STT3B or OST48 was recovered in these pull-downs (Fig. 8D,E). Taken together, we conclude that KCP2 associates specifically with three core OST subunits, STT3A, STT3B and OST48. On the basis of the prominent interaction of KCP2 with newly synthesised STT3A rather than STT3B, we speculate that it is preferentially incorporated into the STT3A-containing isoforms of the OST.

Discussion

This study provides a detailed molecular characterisation of keratinocyte-associated protein 2 (KCP2), and directly addresses

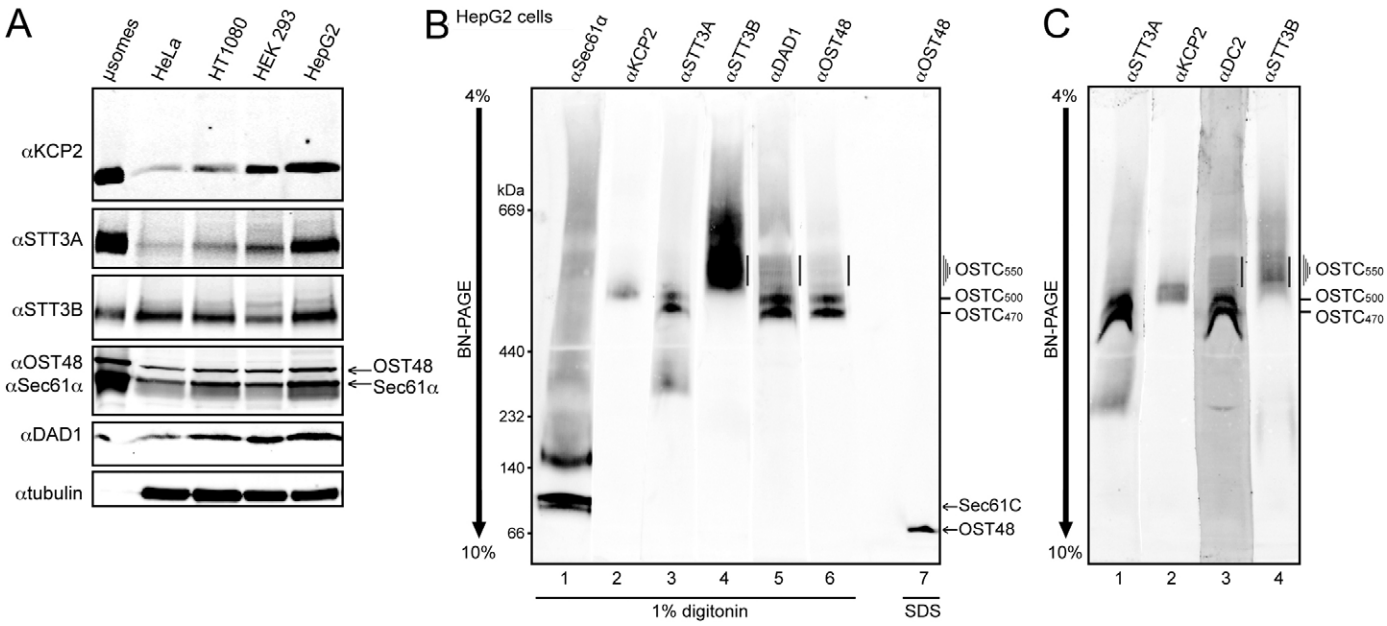

Fig. 7. KCP2 is assembled into distinct isoforms of the OST complex containing STT3A as a catalytic subunit. (**A**) Infrared western blot analysis of RIPA lysates (40 μg total protein per lane) of various cultured cell lines (HeLa, cervical epithelial carcinoma; HT1080, fibrosarcoma breast cancer; HEK293, human embryonic kidney; HepG2, hepatoma) with the anti-KCP2, anti-STT3A, anti-STT3B, anti-OST48, anti-Sec61α and anti-DAD1 antibodies. Alpha-tubulin was detected as a loading control. (**B**,**C**) Infrared western blotting after BN-PAGE analysis of digitonin-solubilised HepG2 cells with antibodies to Sec61α, KCP2, STT3A, STT3B, DAD1, OST48 and DC2 as labelled. The protein complexes containing STT3A (OSTC470 and OSTC500), STT3B (OSTC550) and Sec61α (Sec61C) are indicated at the right.

the proposal by Shibatani et al. that KCP2 is a new subunit of the mammalian OST complex (Shibatani et al., 2005).

Expression of KCP2 by leaky ribosomal scanning

Transient expression of the *KCP2* cDNA in cultured mammalian cells produces two variants of ~15 and ~18 kDa, both of which can be detected by an antibody recognising a C-terminal epitope. The ~15 kDa product is far more prevalent, and inspection of the KCP2 coding region suggested that this polypeptide results from initiation of translation at one of two downstream start codon(s) Met26 and/or Met27 (Fig. 2). Inefficient initiation as a result of leaky ribosome scanning is a well-documented phenomenon that is dependent upon the bases flanking the first AUG codon (Kozak, 1999; Kozak, 2002). The first AUG codon of KCP2 is in a particularly poor context (Fig. 2), and we used the addition of an N-terminal FLAG tag to confirm the origin of the two KCP2-derived species. Interestingly, when endogenous KCP2 was analysed in a variety of cell lines, the ~15 kDa species was clearly the predominant, if not the exclusive, form detected (Fig. 7A and data not shown). Although we cannot formally exclude the possibility that this major KCP2 species results from the proteolytic processing of a longer form, our results indicate that the Met27 codon of human *KCP2* mRNA is the principal site of translation initiation, and we conclude that this is most probably the case for the majority of vertebrates (supplementary material Fig. S2) (see also Bazykin and Kochetov, 2011; Kochetov, 2005).

KCP2 has three TM spans and a C-terminal ER retention signal

Elucidating membrane protein topology is an important step towards understanding structure and function, and we have used a well-established protease protection assay to address this issue. Our results clearly indicate that FLAG–KCP2 has an N_{lum}-C_{cyt} topology and therefore an odd number of TM segments. Likewise the endogenous, untagged, KCP2 protein also has a cytosolic C-terminus. These data strongly support a model for KCP2 with three TM spans (Figs 1, 3), and rule out an alternative model with four TM spans (cf. Shibatani et al., 2005) that results from the unusual length of the final TM span (Cuthbertson et al., 2005). Our immunofluorescence studies show that KCP2 is an ER resident protein (Fig. 4B and Fig. 5A), and our topology analysis shows that its C-terminal KKxx motif is cytosolic and could hence contribute to this subcellular localisation (Harter and Wieland, 1996; Teasdale and Jackson, 1996). Using FLAG–KCP2 or a version where the putative KKxx signal has been mutated, we find that this motif does contribute to the retrieval of overexpressed KCP2 from post-ER locations (Fig. 5), presumably through its interaction with COPI coat components (Cosson and Letourneur, 1994). Given the association of KCP2 with OST complexes (see below), the KKxx motif of KCP2 might act, together with other OST subunits, to ensure the steady state residency of the OST complex in the ER (cf. Fu and Kreibich, 2000).

Association of KCP2 with the mammalian OST complex

Purification of canine OST revealed two distinct isoforms that contained ribophorin I, ribophorin II, OST48, DAD1 and either STT3A or STT3B (Kelleher et al., 2003). Subsequent BN-PAGE analysis identified a stable ~500 kDa OST complex, purified through its association with ER bound ribosomes, that contained STT3A, ribophorin I, ribophorin II, OST48 and DAD1, together with two additional components, KCP2 and DC2 (Shibatani et al., 2005). STT3B-containing OST complexes were not reported in

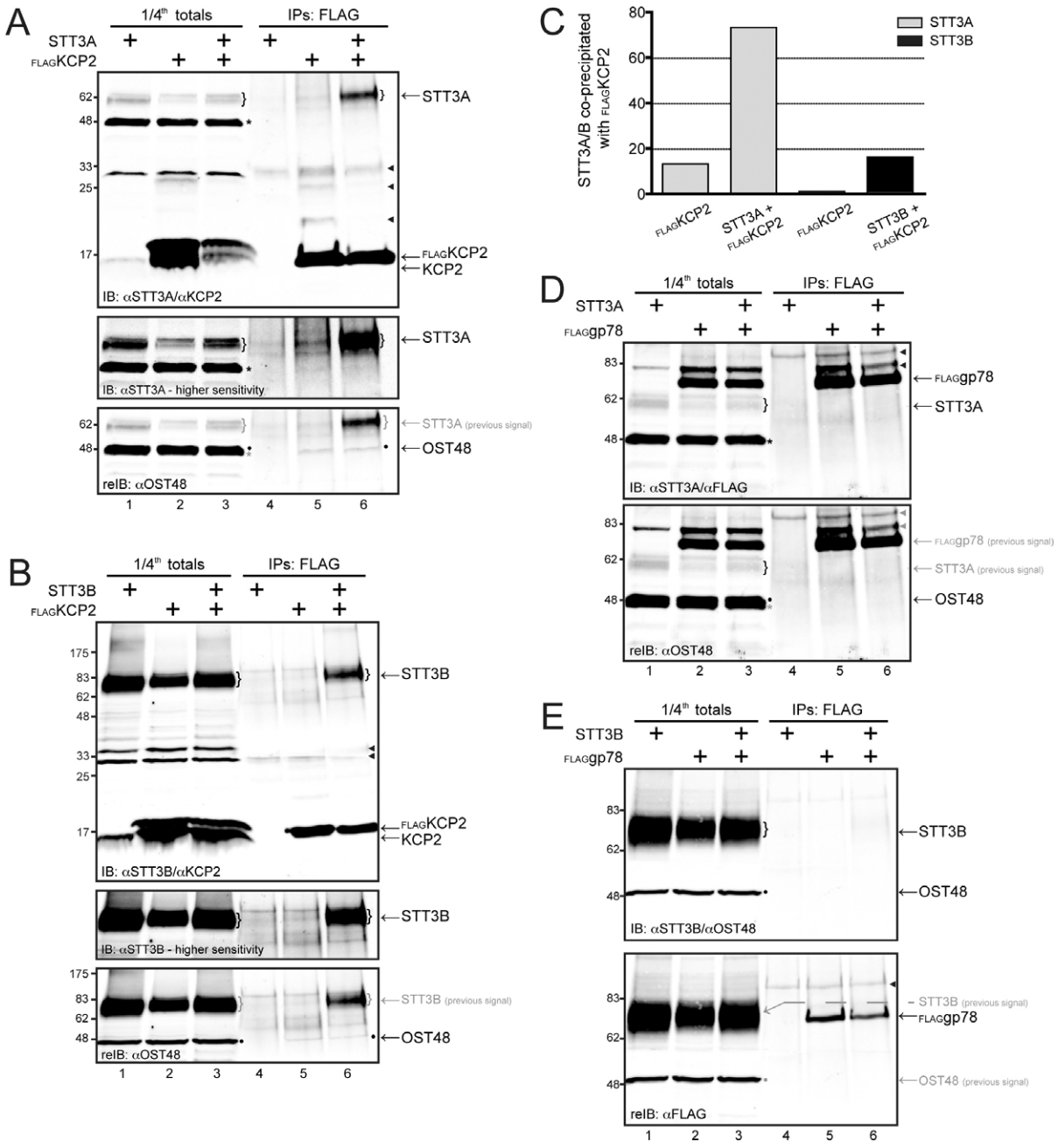

Fig. 8. FLAG–KCP2 is associated specifically with core OST subunits. (**A**,**B**,**D**,**E**) HEK293 cells were (co-)transfected with expression plasmids for the proteins indicated, and digitonin lysates were immunoprecipitated with mouse anti-FLAG. One quarter of the total lysate used for each immunoprecipitation reaction (lanes 1–3) and the immunopurified proteins (lanes 4–6) were analysed by immunoblotting (IB) with the antibodies indicated, followed by re-immunoblotting for additional components (reIB). When detecting the endogenous OST48 signal (A,B,D) or the FLAG–gp78 signal (E), the earlier signals could still be seen in totals and in anti-FLAG precipitates (indicated in grey lettering). In A and D, a non-specific band always detected in total lysate samples by the anti-STT3A antibody is indicated by asterisks. This non-specific immunoreaction product migrates in the vicinity of OST48, which is marked by black circles for clarity. Cross-reacting bands occasionally detected by the anti-KCP2 or anti-FLAG antibodies are indicated by arrowheads. (**C**) The graph shows the relative amount of FLAG–KCP2-interacting STT3A (grey bars) and STT3B (black bars). The levels of STT3A and STT3B in the immunoprecipitates were expressed relative to the corresponding total levels, and then normalised to the levels of the recovered FLAG–KCP2 in the same samples.

the study by Shibatani et al. (Shibatani et al., 2005), consistent with the comparatively loose association of STT3B with the ribosome-associated membrane protein fraction (Fig. 6) (see also Ruiz-Canada et al., 2009). In the present study, we have analysed digitonin-solubilised HepG2 cell extracts by BN-PAGE and immunoblotting to minimise disruption and detect endogenous OST complexes (Schagger et al., 1994; Wittig et al., 2006). Two STT3A-containing complexes of ~470 kDa (OSTC470) and ~500 kDa (OSTC500), and a larger STT3B-containing complex of a heterologous nature (OSTC550) were detected (Fig. 7B). All three of these species appear to contain OST48, DAD1, ribophorin I and ribophorin II (Fig. 7B and data not shown),

consistent with previous studies (Kelleher et al., 2003; Shibatani et al., 2005). We show here that the putative OST subunit, DC2, also co-migrates with all three of these OST species (Fig. 7C), suggesting that it assembles with all of these complexes. By contrast, KCP2 is the only protein analysed in this study that seems to assemble only with the larger of the two STT3A-containing complexes defined here (OSTC500; Fig. 7B,C), providing a physical distinction between the two complexes (cf. Shibatani et al., 2005; Wang and Dobberstein, 1999). Furthermore, our BN-PAGE analysis indicated that KCP2 might not be a prominent component of the STT3B-containing OST complex (Fig. 7B,C).

At a qualitative level, the expression patterns of both KCP2 mRNA and protein appear high in cells and tissues that are active in glycoprotein secretion and reflect the expression of STT3A more closely than STT3B (this study) (see also Bonkobara et al., 2003; Kelleher et al., 2003). Until this study, the possibility of an interaction between KCP2 and known components of the mammalian OST complex had not been directly addressed. Therefore, we have used a co-immunoprecipitation approach (Fig. 8) to investigate the physical association of KCP2 with core OST subunits. We found compelling evidence for a specific interaction between KCP2 and STT3A when both are exogenously expressed in HEK293 cells. We also observed an association of KCP2 with STT3B under similar experimental conditions, although quantitative analysis indicates that KCP2 interacts preferentially with exogenous STT3A (Fig. 8C). Likewise, we detected a specific association between FLAG–KCP2 and endogenous STT3A but not with STT3B (Fig. 8C), despite both STT3 isoforms being expressed at comparable levels in HEK293 cells (Fig. 7A). Although less pronounced, there is also evidence of an association between FLAG–KCP2 and OST48. This interaction is not enhanced by overexpression of STT3A or STT3B, and we conclude that either the association of KCP2 with OST48 is independent of the two catalytic subunits, or the levels of endogenous OST48 are limiting under these experimental conditions. Given that yeast OST48 has extensive contacts with most OST subunits (Yan et al., 2003; Yan et al., 2005), we favour the latter possibility. On the basis of these findings, we propose that KCP2 is predominantly incorporated into STT3A-containing OST complexes, but is also associated with at least a subset of the STT3B-containing complexes.

In general terms, STT3A-containing OST complexes appear to favour co-translational *N*-glycosylation, whereas STT3B-containing complexes are more competent for post-translation glycosylation of selected sequons (Ruiz-Canada et al., 2009). Interestingly, with the exception of *Dictyostelium discoideum* that alternates between unicellular and multicellular forms, unicellular eukaryotes do not express a KCP2 homologue that can be identified by sequence similarity (cf. supplementary material Fig. S2). We therefore speculate that the role of KCP2 is associated with some aspect of STT3A function related to the complexity of *N*-glycosylation in multicellular eukaryotes.

Materials and Methods

Antibodies and plasmids

Rabbit polyclonal antibodies recognising KCP2 and STT3B were custom-made by Cambridge Research Biochemicals (Cleveland, UK). The anti-KCP2 antibodies were raised against synthetic peptides from the mouse sequence and affinity purified using a peptide representing residues 208–220 in the conserved C-terminal domain (Fig. 1, underlined sequence). Polyclonal antibodies specific for OST48, DAD1 and STT3A were as previously described (Wilson and High, 2007; Wilson et al., 2008). Monoclonal anti-STT3A was from Abnova (Taipei, Taiwan). Monoclonal anti-FLAG (M2), polyclonal anti-FLAG and polyclonal anti-CNX were purchased from Sigma. The remaining antisera were generous gifts: anti-tubulin (Keith Gull, University of Oxford), anti-Sec61α (Richard Zimmermann, Saarland University, Germany), anti-ribophorin I (Natale-Erwin Ivessa, University of Vienna, Austria), anti-Grp94 (Chris Nicchitta, Duke University Medical Centre, USA), anti-Rpl17 (Martin Pool, University of Manchester) and anti-TGN46 (Vas Ponnambalam, University of Leeds).

Human KCP2 expression plasmids were from OriGene Technologies (Rockville, MD, USA). DNA sequencing verified the presence of a full-length KCP2 insert in pCMV6-AC-Met1KCP2 and a KCP2 insert lacking the first 25 residues in pCMV6-XL4-Met26/27KCP2. Two rounds of PCR were performed to introduce the FLAG epitope tag immediately after the natural initiator methionine, Met1, and the final product was integrated into pcDNA5-FRT-V5-His-TOPO vector with the native stop codon to create Met1 FLAG–KCP2. Using pCMV6-XL4-Met26/27KCP2 as a template, QuikChange site-directed mutagenesis (Agilent Technologies, Stockport, UK) was performed to generate the Met26Ile mutation. For the insertion of the FLAG tag immediately after Met27, the resulting construct pCMV6-XL4-Met27KCP2 was used as a template for PCR. The FLAG–KCP2 SSRN mutant was made by two sequential QuikChange site-directed mutagenesis reactions using pCMV6-XL4-Met27FLAGKCP2 as a template. All constructs were confirmed by DNA sequencing.

The plasmid encoding STT3A was purchased from OriGene Technologies. Plasmids encoding FLAG–gp78 and mouse STT3BFLAG– were kindly provided by Ivan Robert Nabi (University of British Columbia, Vancouver, Canada) and Claude Perreault (University of Montreal, Quebec, Canada), respectively. QuikChange mutagenesis was performed in order to introduce the native stop codon of mouse STT3B, thereby removing the C-terminal FLAG tag.

Cell culture and DNA transfection

All the cell lines were grown in DMEM supplemented with 10% foetal bovine serum and 2 mM L-glutamine at 37℃ under 5% CO_2. Cells were transfected with Lipofectamine 2000 (Invitrogen) according to the manufacturer's instructions, and harvested after 20–24 hours.

Western blotting

Proteins were separated by SDS-PAGE and transferred to Immobilon-FL PVDF membrane (Millipore, Watford, UK) for 2.5 hours at 300 mA. Membranes were blocked for 1 hour with 1× blocking buffer (Sigma, Poole, UK) in TBS (10 mM Tris pH 8.0, 150 mM NaCl), then incubated with primary antibodies overnight at 4℃ in 1× TBS and Sigma blocking buffer supplemented with 0.1% Tween 20. Membranes were washed four times for 10 minutes each with TBS containing 0.1% Tween 20 (TBST), then incubated in the dark for 1 hour at room temperature with IRDye 800CW and/or IRDye 680 goat anti-mouse, anti-rabbit IgG (LI-COR Biosciences, Cambridge, UK) diluted 1/5000 in 1× TBST and Sigma blocking buffer containing 0.01% SDS. After four subsequent washes with TBST, proteins were visualised and quantified with the Odyssey Infrared Imaging System (LI-COR Biosciences).

Trypsin protection assay

FLAG–KCP2-expressing HeLa cells were washed twice with PBS, trypsinised and semi-permeabilised with 40 μg/ml digitonin (Calbiochem). The cell pellet was resuspended in assay buffer (110 mM potassium acetate, 2 mM magnesium acetate, 20 mM HEPES-KOH pH 7.2) and treated with 250 μg/ml trypsin (Roche Molecular Biochemicals) at room temperature for 1 hour in the presence or absence of 1% Triton X-100. After inhibition with 1 mg/ml soybean trypsin inhibitor and 1 mM phenylmethanesulfonyl fluoride (PMSF) for 10 minutes on ice, samples were analysed by western blotting.

Immunofluorescence microscopy

Transfected cells on coverslips were fixed with 3% formaldehyde and 0.2% glutaraldehyde for 20 minutes at room temperature. After quenching unreacted aldehyde groups, cell membranes were permeabilised with 0.1% Triton X-100 and 0.05% SDS for 4 minutes at room temperature. Cells were labelled with primary antibodies for 1 hour followed by the corresponding secondary antibodies conjugated to Alexa Fluor 488 or 594 (Molecular Probes) for a further hour. For TGN46 staining, cells were fixed in methanol at –20℃ for 4 minutes. Coverslips were mounted with Mowiol and observed using an Olympus BX60 upright microscope equipped with a CoolSnap ES camera (Roper Scientific) driven by Metamorph software (Universal Imaging Corporation). Images were processed using Adobe Photoshop CS4. All experiments were performed at least twice and resulted in similar labelling patterns. For the experiments shown in Figs 4 and 5, the coverslips were thoroughly inspected and the images displayed are representative of the whole population of transfected cells.

RAMP isolation

The release of proteins from the RAMP fraction was assessed as described by Ruiz-Canada et al. (Ruiz-Canada et al., 2009). Briefly, HeLa cells were solubilised with buffer A (20 mM Tris-HCl pH 7.4, 5 mM $MgCl_2$, 3 mM $MnCl_2$, 12% glycerol, 1 mM dithiothreitol, 1.5% digitonin, 1 mM cycloheximide and 1× protease inhibitor cocktail) adjusted to 25, 75, 150 or 300 mM NaCl at 4℃ for 1 hour. Digitonin lysates were treated with DNase I (60 units) for 10 minutes at 37℃ before being centrifuged for 20 minutes at 270,000 ***g*** in a TLA-120.2 rotor. Supernatants were collected and the RAMP pellet was solubilised in 50 mM Tris-HCl pH 7.4, 0.5% SDS with sonication before analysis by SDS-PAGE and western blotting.

Sample preparation for BN-PAGE

BN-PAGE was based on the protocol of Wittig et al. (Wittig et al., 2006). Fifteen passes through a ball-bearing homogeniser (10 µm clearance) was used to homogenise ~25 mg of sedimented HepG2 cells in 500 µl sucrose buffer (83 mM sucrose, 6.6 mM imidazole-HCl pH 7.0). The pellet obtained from 80 mg wet mass of homogenised cells was solubilised in 35 µl solubilisation buffer (50 mM NaCl, 2 mM 6-aminohexanoic acid, 1 mM EDTA, 50 mM imidazole-HCl pH 7.0) containing 1% digitonin, for 20 minutes at 4℃. Insoluble material was removed by centrifugation at 16,000 ***g*** for 10 minutes at 4℃, and the supernatant was mixed with 1/8 volume of 50% glycerol and 1/40 volume of 5% (w/v) Coomassie Blue G250 (Serva) in 500 mM 6-aminohexanoic acid. Samples were loaded onto a 4–10% polyacrylamide gradient gel (Wittig et al., 2006) and run at 4℃ for ~3 hours at 150 V with cathode buffer B (0.02% Coomassie Blue G250 in 50 mM tricine and 7.5 mM imidazole pH 7.0) and anode buffer (25 mM imidazole pH 7.0). A high molecular mass kit for native electrophoresis (GE Healthcare) provided the standards. Protein complexes separated by BN-PAGE were transferred by wet blotting onto PVDF membranes at 70 V for 70 minutes using BN transfer buffer (50 mM tricine pH 7.0, 7.5 mM imidazole). Membranes were destained with methanol and immunodetection was by western blotting as described above.

Co-immunoprecipitation analysis

Cells were solubilised at 4℃ by a 1 hour incubation with TNM buffer (25 mM Tris-HCl pH 7.4, 150 mM NaCl, 5 mM $MgCl_2$) containing 1 mM PMSF, 2.5 mM *N*-ethylmaleimide, a complete protease inhibitor cocktail and 2% digitonin (Merck Chemicals). Non-solubilised material was removed by centrifugation at 16,000 ***g*** for 10 minutes at 4℃. A portion of the post-nuclear supernatant was mixed directly with SDS sample buffer, and the rest was incubated at 4℃ for 1 hour with 25 µl protein A–Sepharose beads (GenScript) to 'preclear' the lysate. Immunoprecipitations were performed by incubating precleared lysates with specific antibody and 30 µl protein-A–Sepharose beads at 4℃ for 4 hours. Beads were washed three times with TNM buffer containing 0.1% digitonin and denatured with sample buffer at 37℃ for 1 hour. Samples were analysed by SDS-PAGE and western blotting.

Acknowledgements

We thank all those who provided us with antibodies and plasmids. We are grateful to Lydia Wunderley for advice regarding BN-PAGE, Quentin Roebuck for affinity purification of KCP2, and Viki Allan for providing microscopy facilities. We thank Lisa Swanton, Helen Watson and Mark Ashe for critical comments on the manuscript and helpful discussions.

Funding

This work was supported by the Biotechnology and Biological Sciences Research Council [grant number BB/E01979x/1 to P.R. and S.H.].

Note added in proof

A recent study has suggested that KCP2 can influence the γ-secretase dependent processing of the amyloid precursor protein (Wilson et al., 2011).

Supplementary material available online at
http://jcs.biologists.org/lookup/suppl/doi:10.1242/jcs.094599/-/DC1

References

Apweiler, R., Hermjakob, H. and Sharon, N. (1999). On the frequency of protein glycosylation, as deduced from analysis of the SWISS-PROT database. *Biochim. Biophys. Acta* **1473**, 4-8.

Banting, G. and Ponnambalam, S. (1997). TGN38 and its orthologues: roles in post-TGN vesicle formation and maintenance of TGN morphology. *Biochim. Biophys. Acta* **1355**, 209-217.

Bause, E., Wesemann, M., Bartoschek, A. and Breuer, W. (1997). Epoxyethylglycyl peptides as inhibitors of oligosaccharyltransferase: double-labelling of the active site. *Biochem. J.* **322**, 95-102.

Bazykin, G. A. and Kochetov, A. V. (2011). Alternative translation start sites are conserved in eukaryotic genomes. *Nucleic Acids Res.* **39**, 567-577.

Beatson, S. and Ponting, C. P. (2004). GIFT domains: linking eukaryotic intraflagellar transport and glycosylation to bacterial gliding. *Trends Biochem. Sci.* **29**, 396-399.

Bolt, G., Kristensen, C. and Steenstrup, T. D. (2005). Posttranslational N-glycosylation takes place during the normal processing of human coagulation factor VII. *Glycobiology* **15**, 541-547.

Bonkobara, M., Das, A., Takao, J., Cruz, P. D. and Ariizumi, K. (2003). Identification of novel genes for secreted and membrane-anchored proteins in human keratinocytes. *Br. J. Dermatol.* **148**, 654-664.

Chenna, R., Sugawara, H., Koike, T., Lopez, R., Gibson, T. J., Higgins, D. G. and Thompson, J. D. (2003). Multiple sequence alignment with the Clustal series of programs. *Nucl. Acids Res.* **31**, 3497-500.

Chavan, M., Yan, A. and Lennarz, W. J. (2005). Subunits of the translocon interact with components of the oligosaccharyl transferase complex. *J. Biol. Chem.* **280**, 22917-22924.

Cosson, P. and Letourneur, F. (1994). Coatomer interaction with di-lysine endoplasmic reticulum retention motifs. *Science* **263**, 1629-1631.

Cuthbertson, J. M., Doyle, D. A. and Sansom, M. S. (2005). Transmembrane helix prediction: a comparative evaluation and analysis. *Protein Eng. Des. Sel.* **18**, 295-308.

Fu, J. and Kreibich, G. (2000). Retention of subunits of the oligosaccharyltransferase complex in the endoplasmic reticulum. *J. Biol. Chem.* **275**, 3984-3990.

Gorlich, D., Prehn, S., Hartmann, E., Kalies, K. U. and Rapoport, T. A. (1992). A mammalian homolog of SEC61p and SECYp is associated with ribosomes and nascent polypeptides during translocation. *Cell* **71**, 489-503.

Harada, Y., Li, H. and Lennarz, W. J. (2009). Oligosaccharyltransferase directly binds to ribosome at a location near the translocon-binding site. *Proc. Natl. Acad. Sci. USA* **106**, 6945-6949.

Harter, C. and Wieland, F. (1996). The secretory pathway: mechanisms of protein sorting and transport. *Biochim. Biophys. Acta* **1286**, 75-93.

Hebert, D. N., Garman, S. C. and Molinari, M. (2005). The glycan code of the endoplasmic reticulum: asparagine-linked carbohydrates as protein maturation and quality-control tags. *Trends Cell Biol.* **15**, 364-370.

Helenius, A. and Aebi, M. (2004). Roles of N-linked glycans in the endoplasmic reticulum. *Annu. Rev. Biochem.* **73**, 1019-1049.

Hese, K., Otto, C., Routier, F. H. and Lehle, L. (2009). The yeast oligosaccharyl-transferase complex can be replaced by STT3 from Leishmania major. *Glycobiology* **19**, 160-171.

Hirokawa, T., Boon-Chieng, S. and Mitaku, S. (1998). SOSUI: classification and secondary structure prediction system for membrane proteins. *Bioinformatics* **14**, 378-379.

Hofmann, K. and Stoffel, W. (1993). TMbase - a database of membrane spanning proteins segments. *Biol. Chem. Hoppe Seyler* **374**, 166-168.

Izquierdo, L., Schulz, B. L., Rodrigues, J. A., Guther, M. L., Procter, J. B., Barton, G. J., Aebi, M. and Ferguson, M. A. (2009). Distinct donor and acceptor specificities of Trypanosoma brucei oligosaccharyltransferases. *EMBO J.* **28**, 2650-2661.

Karaoglu, D., Kelleher, D. J. and Gilmore, R. (1997). The highly conserved Stt3 protein is a subunit of the yeast oligosaccharyltransferase and forms a subcomplex with Ost3p and Ost4p. *J. Biol. Chem.* **272**, 32513-32520.

Kelleher, D. J. and Gilmore, R. (1997). DAD1, the defender against apoptotic cell death, is a subunit of the mammalian oligosaccharyltransferase. *Proc. Natl. Acad. Sci. USA* **94**, 4994-4999.

Kelleher, D. J. and Gilmore, R. (2006). An evolving view of the eukaryotic oligosaccharyltransferase. *Glycobiology* **16**, 47R-62R.

Kelleher, D. J., Kreibich, G. and Gilmore, R. (1992). Oligosaccharyltransferase activity is associated with a protein complex composed of ribophorins I and II and a 48 kd protein. *Cell* **69**, 55-65.

Kelleher, D. J., Karaoglu, D., Mandon, E. C. and Gilmore, R. (2003). Oligosaccharyltransferase isoforms that contain different catalytic STT3 subunits have distinct enzymatic properties. *Mol. Cell* **12**, 101-111.

Knauer, R. and Lehle, L. (1999). The oligosaccharyltransferase complex from yeast. *Biochim. Biophys. Acta* **1426**, 259-273.

Kochetov, A. V. (2005). AUG codons at the beginning of protein coding sequences are frequent in eukaryotic mRNAs with a suboptimal start codon context. *Bioinformatics* **21**, 837-840.

Kolhekar, A. S., Quon, A. S., Berard, C. A., Mains, R. E. and Eipper, B. A. (1998). Post-translational N-glycosylation of a truncated form of a peptide processing enzyme. *J. Biol. Chem.* **273**, 23012-23018.

Kowarik, M., Numao, S., Feldman, M. F., Schulz, B. L., Callewaert, N., Kiermaier, E., Catrein, I. and Aebi, M. (2006). N-linked glycosylation of folded proteins by the bacterial oligosaccharyltransferase. *Science* **314**, 1148-1150.

Kozak, M. (1991). An analysis of vertebrate mRNA sequences: intimations of translational control. *J. Cell Biol.* **115**, 887-903.

Kozak, M. (1999). Initiation of translation in prokaryotes and eukaryotes. *Gene* **234**, 187-208.

Kozak, M. (2002). Pushing the limits of the scanning mechanism for initiation of translation. *Gene* **299**, 1-34.

Lee, M. C., Miller, E. A., Goldberg, J., Orci, L. and Schekman, R. (2004). Bi-directional protein transport between the ER and Golgi. *Annu. Rev. Cell Dev. Biol.* **20**, 87-123.

Nasab, F. P., Schulz, B. L., Gamarro, F., Parodi, A. J. and Aebi, M. (2008). All in one: Leishmania major STT3 proteins substitute for the whole oligosaccharyltransferase complex in Saccharomyces cerevisiae. *Mol. Biol. Cell* **19**, 3758-3768.

Nikonov, A. V., Snapp, E., Lippincott-Schwartz, J. and Kreibich, G. (2002). Active translocon complexes labeled with GFP-Dad1 diffuse slowly as large polysome arrays in the endoplasmic reticulum. *J. Cell Biol.* **158**, 497-506.

Nilsson, I., Kelleher, D. J., Miao, Y., Shao, Y., Kreibich, G., Gilmore, R., von Heijne, G. and Johnson, A. E. (2003). Photocross-linking of nascent chains to the STT3 subunit of the oligosaccharyltransferase complex. *J. Cell Biol.* **161**, 715-725.

Ohtsubo, K. and Marth, J. D. (2006). Glycosylation in cellular mechanisms of health and disease. *Cell* **126**, 855-867.

Pathak, R., Hendrickson, T. L. and Imperiali, B. (1995). Sulfhydryl modification of the yeast Wbp1p inhibits oligosaccharyl transferase activity. *Biochemistry* **34**, 4179-4185.

Ruiz-Canada, C., Kelleher, D. J. and Gilmore, R. (2009). Cotranslational and posttranslational N-glycosylation of polypeptides by distinct mammalian OST isoforms. *Cell* **136**, 272-283.

Sanjay, A., Fu, J. and Kreibich, G. (1998). DAD1 is required for the function and the structural integrity of the oligosaccharyltransferase complex. *J. Biol. Chem.* **273**, 26094-26099.

Schagger, H., Cramer, W. A. and von Jagow, G. (1994). Analysis of molecular masses and oligomeric states of protein complexes by blue native electrophoresis and isolation of membrane protein complexes by two-dimensional native electrophoresis. *Anal. Biochem.* **217**, 220-230.

Schulz, B. L. and Aebi, M. (2009). Analysis of glycosylation site occupancy reveals a role for Ost3p and Ost6p in site-specific N-glycosylation efficiency. *Mol. Cell Proteomics* **8**, 357-364.

Schulz, B. L., Stirnimann, C. U., Grimshaw, J. P., Brozzo, M. S., Fritsch, F., Mohorko, E., Capitani, G., Glockshuber, R., Grutter, M. G. and Aebi, M. (2009). Oxidoreductase activity of oligosaccharyltransferase subunits Ost3p and Ost6p defines site-specific glycosylation efficiency. *Proc. Natl. Acad. Sci. USA* **106**, 11061-11066.

Shibatani, T., David, L. L., McCormack, A. L., Frueh, K. and Skach, W. R. (2005). Proteomic analysis of mammalian oligosaccharyltransferase reveals multiple subcomplexes that contain Sec61, TRAP, and two potential new subunits. *Biochemistry* **44**, 5982-5992.

Silberstein, S., Collins, P. G., Kelleher, D. J. and Gilmore, R. (1995). The essential OST2 gene encodes the 16-kD subunit of the yeast oligosaccharyltransferase, a highly conserved protein expressed in diverse eukaryotic organisms. *J. Cell Biol.* **131**, 371-383.

Sonnhammer, E. L., von Heijne, G. and Krogh, A. (1998). A hidden Markov model for predicting transmembrane helices in protein sequences. *Proc. Int. Conf. Intell. Syst. Mol. Biol.* **6**, 175-182.

Spirig, U., Bodmer, D., Wacker, M., Burda, P. and Aebi, M. (2005). The 3.4 kDa Ost4 protein is required for the assembly of two distinct oligosaccharyltransferase complexes in yeast. *Glycobiology* **15**, 1396-1406.

te Heesen, S., Knauer, R., Lehle, L. and Aebi, M. (1993). Yeast Wbp1p and Swp1p form a protein complex essential for oligosaccharyl transferase activity. *EMBO J.* **12**, 279-284.

Teasdale, R. D. and Jackson, M. R. (1996). Signal-mediated sorting of membrane proteins between the endoplasmic reticulum and the golgi apparatus. *Annu. Rev. Cell Dev. Biol.* **12**, 27-54.

Wang, L. and Dobberstein, B. (1999). Oligomeric complexes involved in translocation of proteins across the membrane of the endoplasmic reticulum. *FEBS Lett.* **457**, 316-322.

Waterhouse, A. M., Procter, J. B., Martin, D. M., Clamp, M. and Barton, G. J. (2009). Jalview Version 2 - a multiple sequence alignment editor and analysis workbench. *Bioinformatics* **25**, 1189-1191.

Wilson, C. M. and High, S. (2007). Ribophorin I acts as a substrate-specific facilitator of N-glycosylation. *J. Cell Sci.* **120**, 648-657.

Wilson, C. M., Roebuck, Q. and High, S. (2008). Ribophorin I regulates substrate delivery to the oligosaccharyltransferase core. *Proc. Natl. Acad. Sci. USA* **105**, 9534-9539.

Wilson, C. M., Magnaudeix, A., Yardin, C. and Terro, F. (2011). DC2 and keratinocyte-associated protein 2 (KCP2), subunits of the oligosaccharyltransferase complex, are regulators of the gamma-secretase-directed processing of amyloid precursor protein (APP). *J. Biol. Chem.* **286**, 31080-31091.

Wilson, R., Allen, A. J., Oliver, J., Brookman, J. L., High, S. and Bulleid, N. J. (1995). The translocation, folding, assembly and redox-dependent degradation of secretory and membrane proteins in semi-permeabilized mammalian cells. *Biochem. J.* **307**, 679-687.

Wittig, I., Braun, H. P. and Schagger, H. (2006). Blue native PAGE. *Nat. Protoc.* **1**, 418-428.

Yan, A., Ahmed, E., Yan, Q. and Lennarz, W. J. (2003). New findings on interactions among the yeast oligosaccharyl transferase subunits using a chemical cross-linker. *J. Biol. Chem.* **278**, 33078-33087.

Yan, A., Wu, E. and Lennarz, W. J. (2005). Studies of yeast oligosaccharyl transferase subunits using the split-ubiquitin system: topological features and in vivo interactions. *Proc. Natl. Acad. Sci. USA* **102**, 7121-7126.